Research Articles

GREENSUSMATER

Greensusmater
Vol. 3, No. 1, 2026
https://doi.org/10.62755/gsm.2026.04

Check for updates

Design and Optimization of $CsPbI_3$ Perovskite Solar Cells Using SCAPS-1D

Muhamad Kevin Ristiansyah[1], Bayu Prasetya[1], Mochammad Ghulam Isaq Khan[1], Muhammad Yasin Siregar[1], Abyan Abdillah Saoloan Panjaitan[1], Eri Widianto[2], Eka Nurfani[1,3,*]

[1] *Department of Materials Engineering, Faculty of Industrial Technology, Institut Teknologi Sumatera (ITERA), Lampung 35365, Indonesia*
[2] *Department of Physics, Faculty of Engineering, Universitas Singaperbangsa Karawang, Telukjambe Timur, Karawang 41361, Indonesia*
[3] *Center for Green and Sustainable Materials, Institut Teknologi Sumatera (ITERA), South Lampung 35365, Indonesia*

Corresponding author: eka.nurfani@mt.itera.ac.id

ARTICLE HISTORY: Received: April 15, 2026 | Revised: May 8, 2026 | Accepted: May 10, 2026

ABSTRACT

This study investigates the optimization of $CsPbI_3$-based perovskite solar cells using SCAPS-1D simulation with a device structure of FTO/ZnO/$CsPbI_3$/Spiro-OMeTAD/metal. Key parameters, including absorber thickness, defect density, acceptor concentration, and transport layer properties, were systematically analyzed. The results show that absorber thickness significantly affects device performance, with an optimal thickness of 1.6 µm yielding an efficiency of 17.66%. Optimization of defect density and acceptor concentration further enhances device performance. After overall optimization, the power conversion efficiency increases from 16.3% to 23.1%, with V_{oc} improving from 1.19 V to 1.39 V, J_{sc} from 18.33 to 20.5 mA/cm^2, and FF from 75.2% to 87.4%. The improvement is supported by enhanced J–V characteristics and near-unity quantum efficiency over a wide wavelength range. These results demonstrate that parameter optimization plays a crucial role in achieving high-performance $CsPbI_3$ perovskite solar cells.

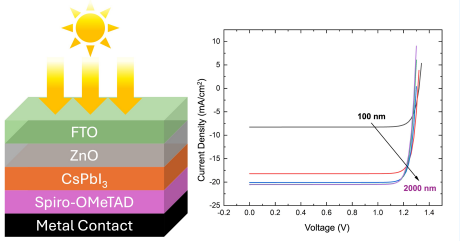

Keywords: *CsPbI3; perovskite; SCAPS-1D; solar cells*

1. INTRODUCTION

Fossil fuels are currently the most widely used energy source. The increasing population also requires high energy needs [1]. Thus, the increasing demand for fossil fuels drives their scarcity. To reduce the use of fossil fuels, technological updates are needed to utilize renewable energy sources, such as solar energy, which has great potential [2]. Furthermore, silicon is the most widely used semiconductor material in solar cell applications. However, production costs for Si-based photovoltaic devices are higher than those of other thin-film technologies, which is a significant drawback for the continuous production of Si-based solar cells.

Therefore, since 2009, perovskite materials have become a choice for use as semiconductors in solar cell systems [3]. Perovskite solar cells have attracted attention because they are relatively inexpensive and easy to manufacture, and their excellent performance has spurred significant research. The efficiency of perovskite solar cells has increased from 3.8% to 25.2% in a short time from 2009 to 2021 [4]. In 2009, perovskite halides were first used as visible-light sensitizers in dye-sensitized solar cells, achieving a power conversion efficiency (PCE) of 3-4%. Perovskite halide shows extraordinary optoelectronic properties, making this semiconductor very good for photovoltaic applications. Perovskite solar cells exhibit good stability, with a PCE of 9.7% reported in 2012. These advancements have driven extensive research into the optoelectronic properties of perovskite materials, particularly their high absorption coefficient, long carrier diffusion length, and tunable bandgap [5].

Among various perovskite materials, organic-inorganic hybrid perovskites such as methylammonium lead iodide ($MAPbI_3$) have been extensively studied due to their high efficiency and excellent light-harvesting capability. In our previous studies, $MAPbI_3$-based perovskite solar cells have been investigated using various optimization approaches, including modification of the electron transport layer via doping [6], control of TiO_2 thickness [7], adjustment of precursor molarity [8], and surface passivation with FAI and MAI [9], which have yielded significant improvements in device performance. Furthermore, precise optical characterization using techniques such as spectroscopic ellipsometry has been identified as a critical factor for the continuous advancement and performance enhancement of these perovskite-based devices [10]. However, despite their promising performance, $MAPbI_3$-based solar cells still suffer from stability issues, particularly under thermal stress and moisture exposure [11,12,13]. To overcome these limitations, researchers have explored all-inorganic perovskite materials such as cesium lead iodide ($CsPbI_3$), which offer improved thermal stability and better resistance to environmental degradation [14,15,16]. $CsPbI_3$ has attracted considerable attention due to its suitable bandgap and potential for high photovoltaic performance.

In developing perovskite solar cells, theoretical optimization can be used to minimize material consumption and fabrication time and to study the effects of various factors. SCAPS-1D is software for simulating one-dimensional solar cells.

Table 1. Physical characteristics of the solar cell layers used for simulation.

Parameters	Spiro-OMeTAD	$CsPbI_3$	ZnO	FTO
Thickness (nm)	170	100–900	50–100	500
Bandgap (eV)	2.9	1.73	3.3	3.5
Electron affinity (eV)	2.2	3.95	3.9	4.0
Dielectric permittivity (relative)	3	6	9	9
Effective density of conduction band ($1/cm^3$)	2.2×10^{18}	1.1×10^{20}	1.0×10^{19}	2.2×10^{18}
Effective density of valence band ($1/cm^3$)	2.2×10^{18}	8.0×10^{19}	1.0×10^{19}	1.8×10^{19}
Electron mobility (cm^2/Vs)	1.0×10^{-4}	1.6×10^{1}	5.0×10^{1}	2.0×10^{1}
Hole mobility (cm^2/Vs)	2.0×10^{-4}	1.6×10^{1}	5	2.0×10^{1}
Donor density N_d ($1/cm^3$)	-	-	5.0×10^{17}	2.0×10^{19}
Acceptor density N_a ($1/cm^3$)	1.3×10^{18}	1.0×10^{15}	-	-
Electron/Hole thermal velocity (cm/s)	1.0×10^{7}	1.0×10^{7}	1.0×10^{7}	1.0×10^{7}
Defect density (cm^{-3})	1.0×10^{15}	2.1×10^{14}	1.0×10^{15}	1.0×10^{18}
References	[19]	[19]	[25]	[26]

This software is widely used to optimize factors affecting the efficiency of perovskite solar cells [17]. Aseena et al. (2020) simulate the optimization of perovskite solar cell layers with different thicknesses [18]. This study shows that maximum efficiency is achieved by optimizing the absorber layer thickness relative to other layers. Another group simulated the performance of $CsPbI_3$ heterojunction perovskite solar cells using SCAPS-1D [19]. Under optimal conditions, the PCE of the $CsPbI_3$ heterostructure increased from 13.1% to 20.2%. Chowdhury et al. simulate the effect of the defect density in the absorber layer on the efficiency of perovskite solar cells [20]. This study explains the detrimental impact of density defects on solar cell performance and how to mitigate this by increasing the absorber layer thickness. Reyes et al. studied the effect of acceptor concentration (N_a) and the absorber layer's defect density on the efficiency of solar cells [21]. This study shows that an increase in N_a can increase the efficiency of the solar cell.

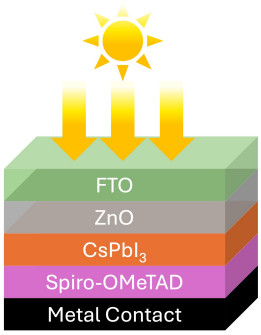

Figure 1. Design of a perovskite solar cell structure.

In this study, the performance of $CsPbI_3$-based perovskite solar cells is systematically investigated using SCAPS-1D simulation. While individual parameter optimizations are common, our study provides a comprehensive simultaneous optimization mapping that specifically focuses on the interplay between the all-inorganic $CsPbI_3$ absorber and the specific combination of ZnO and Spiro-OMeTAD transport layers. We have highlighted how our unique parameter space exploration yields a highly optimized theoretical efficiency, which serves as a robust and necessary benchmark to guide future experimental fabrication of these specific device architectures. The simulation evaluates the effects of key parameters on device performance, including absorber-layer thickness, defect density (N_t), and acceptor concentration (N_a). Furthermore, the influence of transport layers is also analyzed by varying the thickness of the electron transport layer (ETL) and hole transport layer (HTL), as well as the donor density (N_d) of the ETL. In addition, the effect of operating temperature on device performance is examined to assess thermal stability under different conditions. Finally, the overall device performance is evaluated through current density–voltage (J–V) characteristics and quantum efficiency (QE) analysis to provide a comprehensive understanding of the optimized solar cell.

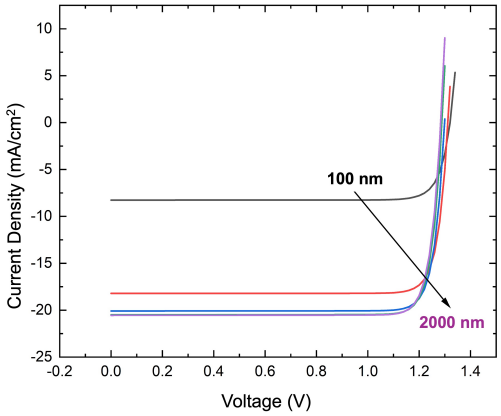

Figure 2. J-V curves with various absorber thicknesses under standard operating temperature (300 K) and AM1.5G illumination condition.

2. METHODS

The material structure is FTO as the transparent conducting oxide (TCO), ZnO as the electron transport layer (ETL), $CsPbI_3$ as the absorber layer, and Spiro-OMeTAD as the hole transport layer (HTL). The composition of the perovskite structure to be optimized is presented in Figure 1. Moreover, Table 1 presents the physical characteristics used in the SCAPS-1D software for numerical analysis. The physical and optical parameters for the ZnO transport layer, such as defect density and electronic transitions, were specifically chosen based on detailed experimental characterizations of spray-fabricated ZnO thin films reported in our previous works [22,23]. Table 2 presents the light source parameters, using the solar radiation spectrum of AM 1.5G, a power density of 100 mW/cm^2, and a working temperature of 300 K [24]. In this study, the parameters varied were the thickness of each layer (absorber, ETL, and HTL), defect density (N_t), acceptor concentration (N_a), donor density, and working temperature.

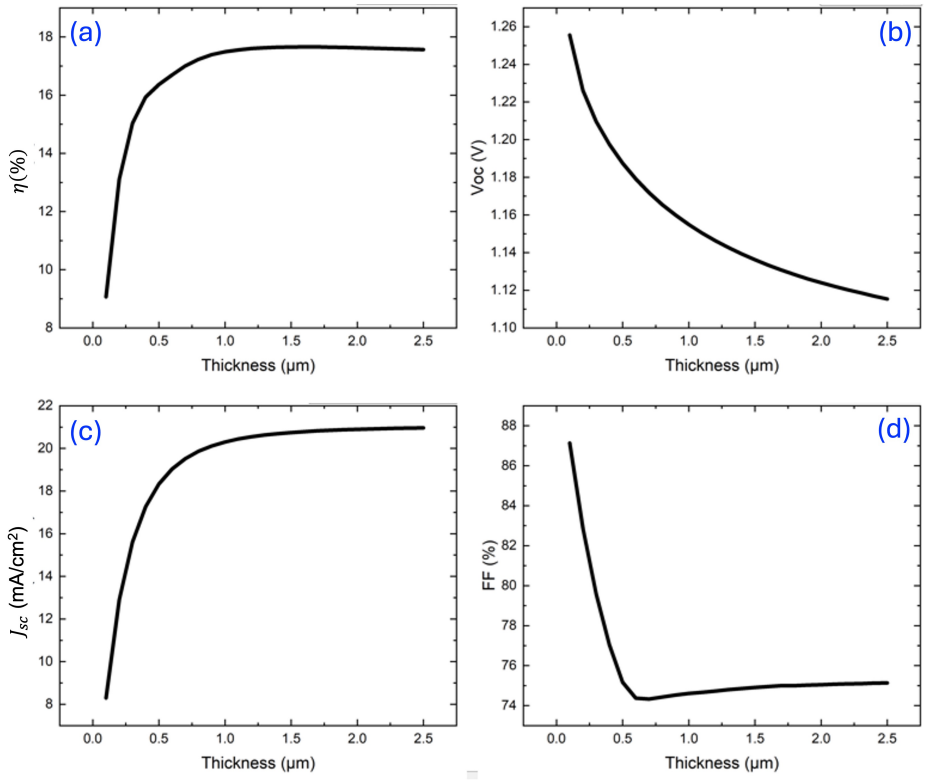

Figure 3. Effect of $CsPbI_3$ thickness on (a) efficiency (η), (b) V_{oc}, (c) J_{sc}, and (d) Fill Factors.

Optimal conditions were strictly defined as the precise combination of physically realistic parameters that maximizes the Power Conversion Efficiency (PCE). Thickness is an important parameter that increases efficiency in increasing current density. Increasing the absorber layer thickness can increase charge-carrier generation by increasing light absorption in the material [18].

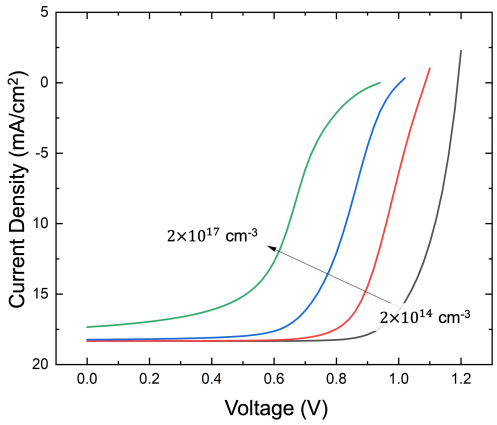

Figure 4. J-V curves with various defect densities (N_t) of $CsPbI_3$ layer.

Acceptor concentration is an important parameter to optimize efficiency, as altering the acceptor concentration primarily modulates the material's electrical conductivity, carrier concentration, and built-in potential (V_{bi}) [21]. Optimal doping shifts the Fermi energy level closer to the valence band, thereby enhancing the built-in electric field (V_{bi}) at the junction, which effectively promotes charge separation and directly boosts the Open Circuit Voltage (V_{oc}). N_t is very important because it can affect the efficiency of the solar cell. Defect density is the number of defects in a material based on a specific energy. Therefore, SCAPS-1D can vary the effect of N_t on the efficiency of the solar cell. Defect density is based on the Shockley-Read-Hall model (Eq. 1):

$$R = \frac{np - n_i^2}{\tau_p(n + n_1) + \tau_n(p + p_1)} \quad (1)$$

where n and p are the electron and hole concentrations obtained by continuity and Poisson equations. The cell characteristics studied are efficiency, J-V characterization, open circuit voltage (V_{oc}), short circuit current (J_{sc}), and Fill Factor (FF). FF is calculated by equating the maximum power (P_{max}) with the theoretical power (P_T) that will produce J_{sc} and V_{oc}. The ratio of energy output to energy input from solar energy is Power Conversion Efficiency (PCE), as in Eqs. 2 and 3 [21]:

$$FF = \frac{P_{max}}{J_{sc} \times V_{oc}} \quad (2)$$

$$\text{PCE}\,(\%) = \frac{V_{oc} \times J_{sc} \times FF}{P_{in}} \times 100 \quad (3)$$

3. RESULTS AND DISCUSSIONS

3.1 Validation of simulation

Before proceeding with the detailed parameter optimization, the baseline simulation results of our unoptimized $CsPbI_3$ solar cell model were compared with experimental data of similar $CsPbI_3$ architectures available in recent literature. This direct comparison demonstrates that our initial model parameters yield highly realistic device performance metrics,

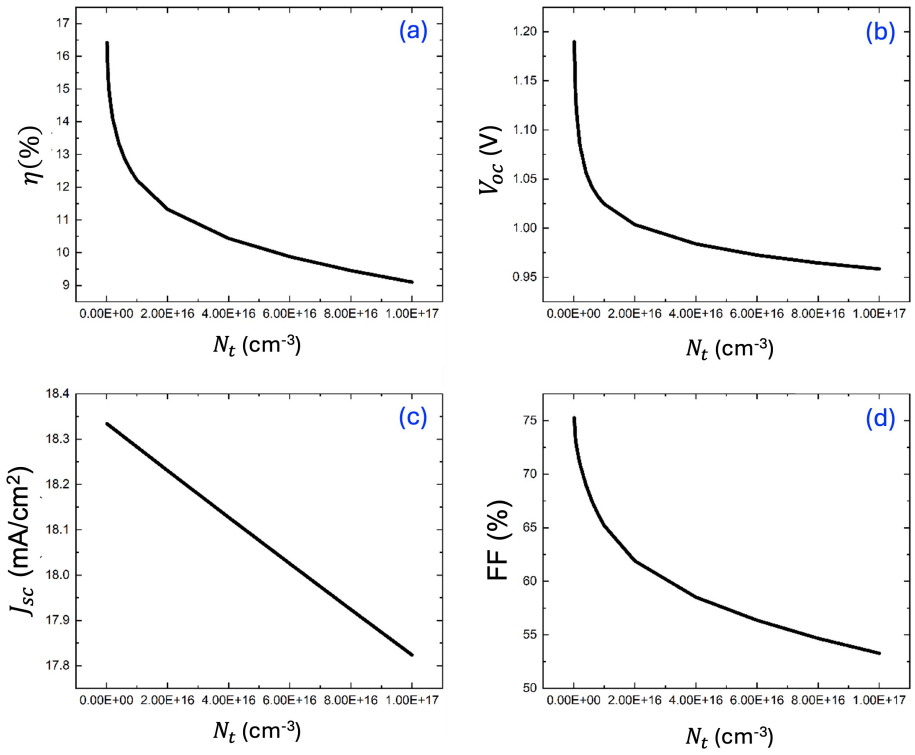

Figure 5. The efficiency (η), V_{oc}, J_{sc}, and FF with various defect density (N_t) of absorber.

thereby validating the fundamental physical models and material definitions utilized within our SCAPS-1D simulation framework.

3.2 Thickness of absorber layer

Figure 2 is the J-V curve obtained from the simulation. Figure 3 shows the simulation results for the effect of the absorber layer thickness on efficiency (PCE), V_{oc}, J_{sc}, and FF with a thickness variation of 100–2000 nm. As the absorber layer thickness increases, efficiency increases, reaching a maximum of 17.66% at 1600 nm. The $CsPbI_3$ material reaches its fundamental absorption depth limit around 1 μm, meaning it absorbs nearly all incident photons with energies above its bandgap. Consequently, increasing the thickness beyond this optimal point does not significantly contribute to additional photogeneration, but instead unnecessarily increases the travel distance for charge carriers, which subsequently raises the probability of non-radiative recombination before they can be effectively collected at the electrodes. This correlation between device efficiency and absorber thickness is inherently non-linear. The non-linearity arises from the fundamental physical competition between two opposing processes within the semiconductor: the generation of charge carriers and their subsequent recombination. Initially, the rapid increase in efficiency is heavily dominated by enhanced photon absorption and carrier generation; however, as the thickness continues to grow, the recombination rate begins to dominate due to longer carrier transit times, causing the efficiency curve to flatten and eventually decline [27]. Therefore, finding the optimal absorber thickness is necessary to achieve a good balance between light absorption and charge-carrier transport [28,29].

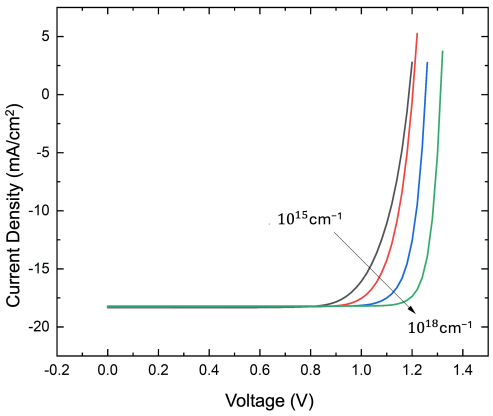

Figure 6. J-V curve of perovskite solar cells with various N_a.

Moreover, the increase in absorber thickness causes the V_{oc} value to decrease. This decrease occurs because the reverse saturation current increases as charge accumulates on the electrodes. When charge builds up on the electrodes, current can no longer flow through the device. The value of J_{sc} increases with thickness because the spectral response at longer wavelengths increases with thickness. The increase in electron-hole pairs is related to photon absorption. Therefore, J_{sc} increases with the absorber thickness. The value of the Fill Factor (FF) also decreased. This occurred due to photon absorption and charge-carrier recombination. The optimum thickness value to achieve maximum efficiency is obtained at a thickness of 1.6 μm with a PCE value of 17.66%, a V_{oc} value of 1.13 Volts, a J_{sc} value of 20.79 mA/cm^2, and FF of 74.96%.

Furthermore, it is important to contrast this theoretically optimized thickness of 1.6 μm with typical experimental

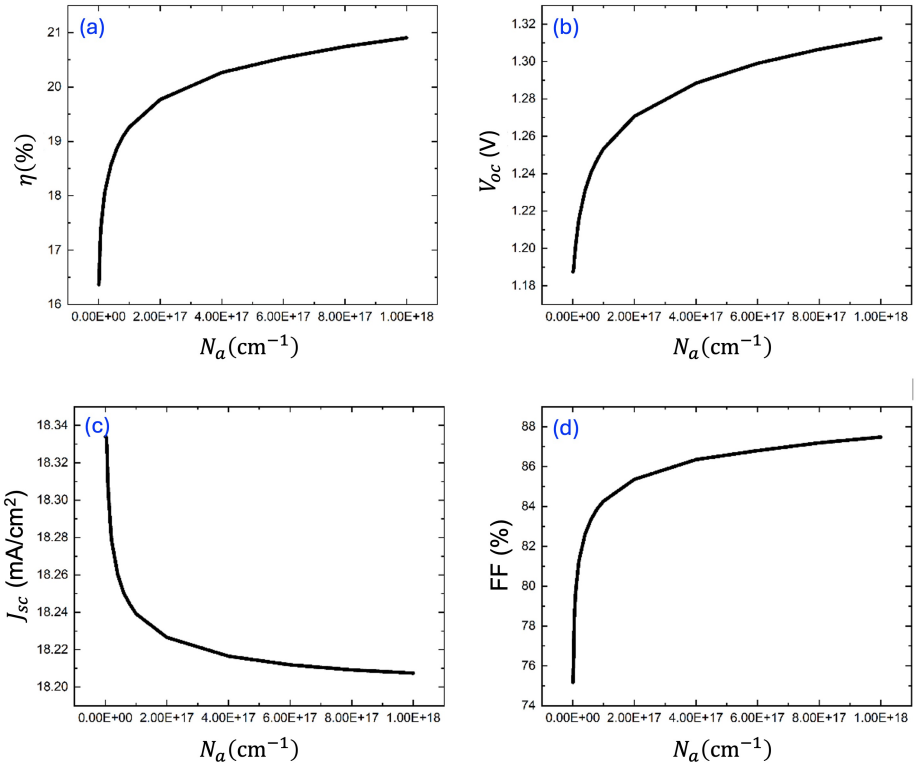

Figure 7. The efficiency, V_{oc}, J_{sc}, and FF of solar cells with various N_a values.

data. In practical device fabrication, the optimal thickness for $CsPbI_3$ absorber layers is frequently found to be significantly lower, typically in the range of 300 to 500 nm [15,16]. This discrepancy arises because our ideal SCAPS-1D simulation does not fully account for the macroscopic morphological defects, severe strain accumulation, and high series resistance that typically plague experimentally deposited perovskite films when their thickness exceeds 500 nm. Thus, while our simulation identifies the fundamental optical limit for maximum photogeneration, practical fabrication must balance optical absorption against the severe morphological deterioration associated with thick films.

Table 2. Light source parameters.

Spectrum	AM 1.5G solar spectrum
Wavelength (nm)	200–4000
Transmission %	100
Ideal light current $G(x)$ (mA/cm^2)	20
Transmission attenuation filter %	100
The ideal light current cell (mA/cm^2)	0

Table 3. A change in solar cell parameters after optimization.

Parameters	Unoptimized	Optimized
PCE (%)	16.3	23.1
V_{oc} (V)	1.19	1.39
J_{sc} (mA/cm^2)	18.33	20.5
FF (%)	75.2	87.4

3.3 Defect density of absorber layer

The absorber defect density strongly influences the solar cell efficiency. Photoelectrons are produced when the absorber layer interacts with light. As the absorber thickness increases, efficiency increases, but defect density also increases, thereby increasing recombination. PCE, V_{oc}, J_{sc}, and FF values decreased when the N_t value of the absorber was increased from 10^{14} to 10^{17} cm^{-3}. The PCE decreased from 16.4% to 9.1% due to non-radiative Shockley-Read-Hall (SRH) recombination [30,31,32], carrier recombination [30,33], and device performance degradation [34,35,36]. Higher defect states act as active recombination centers deep within the bandgap, which severely diminishes the minority carrier lifetime and diffusion length according to Shockley-Read-Hall (SRH) statistics. One way to reduce the value of N_t is by using an ETL layer. This ETL layer can prevent direct reactions between the perovskite absorber and the electrode and can also increase the crystallinity of the perovskite absorber. After optimization, an efficiency of 16.4%, V_{oc} 1.19 V, J_{sc} 18.33 mA/cm^2, and FF = 75.27% are obtained. Comparatively, while our simulation demonstrates that reducing the defect density to 10^{14} cm^{-3} maximizes performance, typical experimental $CsPbI_3$ films exhibit defect densities in the range of 10^{15} to 10^{16} cm^{-3} due to inherent iodine vacancies and imperfect crystallization [15,16]. Achieving the theoretically optimal 10^{14} cm^{-3} level in practical devices remains a significant challenge that requires advanced surface passivation and controlled crystallization techniques.

3.4 Acceptor concentration (N_a) of absorber layer

Figure 6 and Figure 7 result from simulating a $CsPbI_3$-based solar cell by varying the N_a value from 10^{15} cm^{-3} to 10^{18} cm^{-3}. There is an increase in the PCE, V_{oc}, and FF values

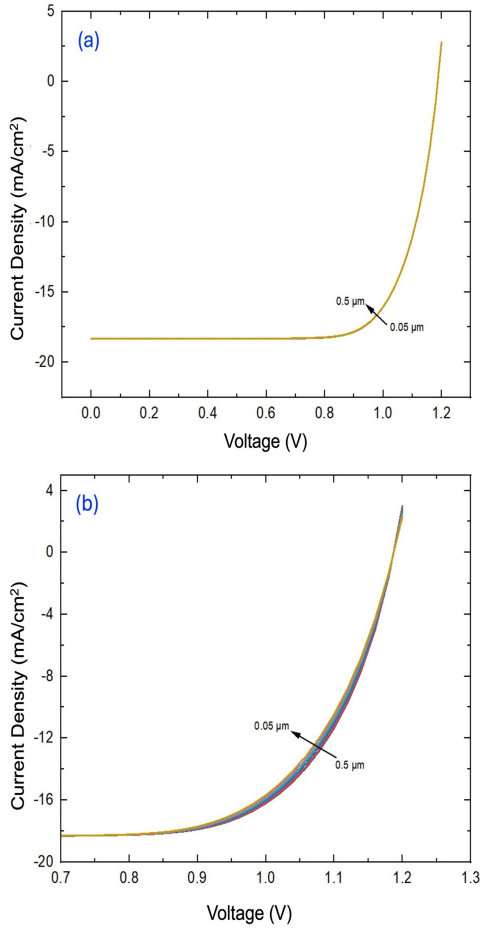

Figure 8. J-V curve as a function of (a) ZnO and (b) Spiro-OMeTAD thickness.

and a decrease in the J_{sc} value when the N_a value increases. When the N_a value is increased, there is a decrease in the energy level of the hole, which increases the V_{oc} value. This increase also occurs because the built-in potential increases. This increases the value of V_{oc} because the charge separation also increases. The optimal N_a value was obtained (10^{18} cm^{-3}) with an efficiency value of 20.90%, V_{oc} = 1.31 V, J_{sc} = 18.21 mA/cm^2, and FF = 87.48%. It is worth noting that experimentally achieving such a high intentional doping concentration of 10^{18} cm^{-3} without inducing structural disorder or secondary non-perovskite phases is highly challenging. Most experimental high-efficiency $CsPbI_3$ devices rely on unintentional self-doping or mild extrinsic doping that reaches approximately 10^{16} cm^{-3} to 10^{17} cm^{-3} [16]. Therefore, this theoretical optimum serves as an upper bound, highlighting the potential gains if highly effective, non-destructive doping strategies can be experimentally realized.

3.5 Thickness of ETL and HTL

ETL is an important layer that reduces recombination losses and should exhibit high optical transmittance to allow efficient light absorption in the perovskite layer. The ZnO thickness varied from 50 to 500 nm. Figure 8(a) shows how ETL thickness affects efficiency, V_{oc}, J_{sc}, and FF. There was an insignificant decrease in V_{oc}, J_{sc}, FF, and PCE with increasing ETL thickness. The thickness of the ETL partially absorbs light, inhibiting the rate of charge generation and collection. This decrease in performance can also result from a reduction in transmittance. The thickness of Spiro-OMeTAD was varied from 50 to 500 nm to find the optimal value, as shown in Figure 8(b). As with ETL thickness variations, no significant influence was observed during HTL thickness modulation. Therefore, the HTL thickness was chosen to be 170 nm for further optimization, which was the initial setting of this study. The thinner the ETL and HTL layers, the higher the efficiency value. The HTL layer needs to be thicker than the ETL layer to reduce the possibility of recombination, as it facilitates prompt transport of the same number of charge carriers to the terminal.

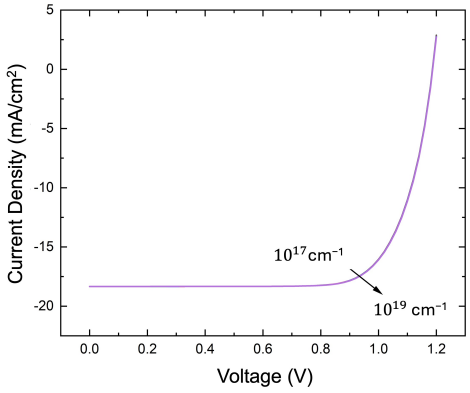

Figure 9. J-V curves with various donor concentrations (N_d) of ZnO.

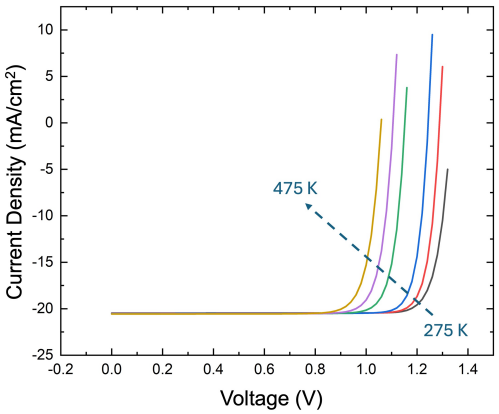

Figure 10. J-V curves with various working temperatures.

Thicker HTL than ETL can make the light-absorbing layer more capable of absorbing photons. These simulated optimal ranges—approximately 50 nm for the ZnO ETL and 170 nm for the Spiro-OMeTAD HTL—are in excellent agreement with state-of-the-art experimental fabrications. In high-efficiency experimental $CsPbI_3$ solar cells, the ETL is typically deposited at thicknesses around 30–50 nm to minimize series resistance, while the HTL is coated at 150–200 nm to ensure complete coverage of the rough perovskite surface while maintaining efficient hole extraction [15,19].

3.6 Donor density (N_d) of ETL

Figure 9 shows the influence of the donor concentration (N_d) of the ETL layer with variations of $10^{17} - 10^{19}$ cm^{-3}. The results obtained are similar to the results of variations in the

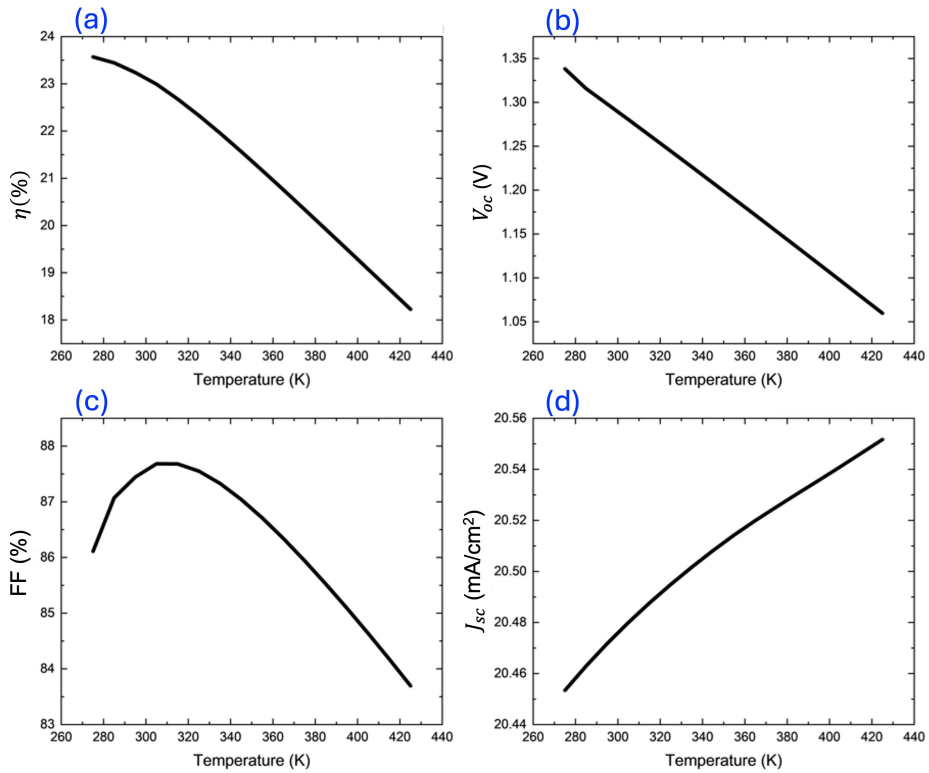

Figure 11. Effect of working temperature on the (a) efficiency, (b) V_{oc}, (c) J_{sc}, and (d) FF.

acceptor concentration of the absorber, where there is an increase in the efficiency, V_{oc}, and FF values and a decrease in the J_{sc} value. However, the N_d variation did not experience a significant increase or decrease, so it did not significantly affect the performance of the $CsPbI_3$ perovskite solar cell. The optimum value of N_d is 10^{19} cm^{-3} because the N_d value must be greater than the N_a value. After all, the greater the donor concentration, the more free electrons, so that it can absorb photons with an efficiency value of 16.38%, $V_{oc} = 1.19$ V, $J_{sc} = 18.33$ mA/cm^2, and FF=75.20%. This optimally simulated donor density of 10^{19} cm^{-3} aligns perfectly with experimental realities. ZnO thin films intrinsically possess a high concentration of shallow donor states, primarily arising from oxygen vacancies and interstitial zinc atoms, which typically yield carrier concentrations in the 10^{18} to 10^{19} cm^{-3} range [25]. Thus, our simulation accurately reflects the inherent electrical properties of experimental ZnO ETLs.

3.7 Working temperature

Figure 10 and Figure 11 present the effect of operating temperature (275–475 K) on the photovoltaic performance of the $CsPbI_3$-based perovskite solar cell, including the J-V characteristics and key parameters such as efficiency (PCE), open-circuit voltage (V_{oc}), short-circuit current density (J_{sc}), and fill factor (FF). While standard testing conditions are near room temperature (300 K), deployed solar cells in real-world applications often operate at significantly elevated temperatures under concentrated sunlight or in hot, arid climates, easily reaching 350 K or more. Therefore, simulating temperatures up to 475 K is absolutely critical for rigorously evaluating the extreme thermal stability limits of the $CsPbI_3$ device and understanding the failure mechanisms associated with increased intrinsic carrier concentrations and enhanced phonon scattering. As the temperature increases, a clear degradation in device performance is observed, with efficiency, V_{oc}, and FF decreasing significantly, while J_{sc} shows a slight increase. The reduction in V_{oc} with increasing temperature is primarily attributed to an increase in intrinsic carrier concentration, which enhances the reverse saturation current. This leads to higher recombination rates and a reduction in the quasi-Fermi level splitting, ultimately lowering the open-circuit voltage. Since V_{oc} is highly sensitive to recombination, it becomes the most affected parameter under elevated temperatures. The fill factor (FF) also decreases with temperature due to increased carrier scattering and recombination losses, as well as degraded diode quality. Higher temperatures can reduce carrier mobility and increase resistive losses, which contribute to a less ideal J-V curve shape.

In contrast, J_{sc} slightly increases with temperature. This behavior can be attributed to the narrowing of the semiconductor bandgap at higher temperatures, which allows the absorption of lower-energy photons, thereby increasing the photogenerated current. However, this improvement is relatively small compared to the losses in V_{oc} and FF. As a result, the overall efficiency decreases with increasing temperature, since the reduction in V_{oc} and FF dominates over the slight increase in J_{sc}. The J-V curves further confirm this trend, where the curve shifts toward lower voltage as temperature increases, indicating a reduction in V_{oc} and degradation in device performance. Overall, these results highlight that temperature is a critical factor affecting the stability and performance of perovskite solar cells. The degradation at higher temperatures is mainly governed by increased recombination, bandgap narrowing, and deterioration of diode characteristics rather than defect generation alone. From an experimental perspective, prolonged exposure to temperatures

approaching 400 K can trigger a detrimental phase transition in $CsPbI_3$, where the photoactive black perovskite phase (α or γ) degrades into the non-photoactive yellow phase (δ) [15,16]. While our simulation captures the electronic degradation mechanisms such as enhanced recombination and intrinsic carrier generation, practical device failure at these elevated temperatures is often dominated by this structural instability, underscoring the critical need for phase-stabilization engineering in real-world applications.

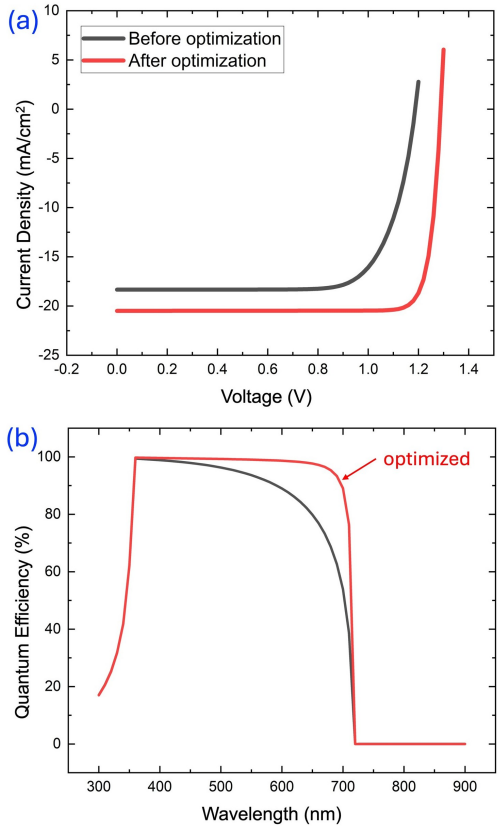

Figure 12. Unoptimized versus optimized (a) J-V Characteristic and (b) quantum efficiency.

3.8 Optimized J–V characteristic and quantum efficiency (QE)

Before optimizing the $CsPbI_3$ perovskite solar cell device, the efficiency was 16.4%, the V_{oc} value was 1.19 V, the J_{sc} value was 18.34 mA/cm^2, and the FF value was 75.2%. After optimization of the FTO/ZnO/$CsPbI_3$/Spiro-OMeTAD device, the thickness and N_a were from 0.5 μm to 1.6 μm and 10^{15} to 10^{18} cm^{-3}. The N_d value of ETL was optimized from 10^{17} to 10^{19} cm^{-3}. After final optimization, efficiency increased to 23.1%, V_{oc} to 1.39 V, J_{sc} to 20.5 mA/cm^2, and FF 87.4%. Figure 12 shows the comparison of the J-V curve and quantum efficiency before and after optimization. Detail of optimized parameters is summarized in Table 3. The theoretically optimized PCE of 23.1% provides a compelling target for future experimental efforts. Currently, the record experimental efficiency for all-inorganic $CsPbI_3$ solar cells hovers around 20–21% [16]. The gap between our theoretical limit and current experimental records suggests that while significant progress has been made, there remains substantial room for improvement through rigorous control of interface energetics, suppression of deep-level defects, and precise tailoring of charge transport layer properties as guided by our simulation.

It is seen that as the voltage increases, current density also increases, and the correlation between wavelength and QE is optimized. QE is the ratio of the number of charge carriers produced photoelectrically to the number of photons entering the solar cell. The QE value increases when the wavelength is 300-710 nm. The highest QE is found in ~360 nm (100%). The QE is gradually decreased by shifting the wavelength to ~710 nm. After optimization, the QE value is almost maximum (100%) in the 300-710 nm range.

4. CONCLUSION

In this study, $CsPbI_3$-based perovskite solar cells were successfully optimized using SCAPS-1D simulation. The results demonstrate that absorber thickness, defect density, and acceptor concentration are critical parameters influencing device performance. An optimal absorber thickness of 1.6 μm provides efficient light absorption and carrier collection. Reducing defect density minimizes recombination losses, while appropriate acceptor concentration enhances charge transport within the absorber layer. After simultaneous optimization of all parameters, the device performance significantly improved, with power conversion efficiency increasing from 16.3% to 23.1%, accompanied by significant enhancements in V_{oc} (from 1.19 V to 1.39 V), J_{sc} (from 18.33 to 20.5 mA/cm^2), and fill factor (from 75.2% to 87.4%). The improved performance is supported by better J-V characteristics and near-unity quantum efficiency across a broad wavelength range. These findings confirm that systematic parameter optimization, using physically realistic parameters grounded in experimental characterization, is an effective strategy to enhance the performance of $CsPbI_3$ perovskite solar cells and provide a robust theoretical benchmark for the design of high-efficiency perovskite-based photovoltaic devices.

ACKNOWLEDGMENTS

This research is supported by the Ministry of Higher Education, Science, and Technology of the Republic of Indonesia (contract no. 172/C3/DT.05.00/PL-BARU/2026 and 1416b/DST/IT9.2.1/PT.01.03/2026) via "Penelitian Terapan-Luaran Prototipe 2026" scheme.

DATA AVAILABILITY STATEMENT

The data that support the findings of this study are available from the corresponding author upon reasonable request.

CONFLICT OF INTEREST

The authors declare that they have no known competing financial interests or personal relationships that could have appeared to influence the work reported in this paper.

REFERENCES

[1] Herna H., Lutfi F., Tambunan E. N. T., Meinarti Y., Rini A. S.. Perovskite solar cells yang stabil udara dan efisien menggunakan nanostruktur ZnO sebagai elektron transport material. *Komunikasi Fisika Indonesia*. 2022;19:75-82. doi:10.31258/jkfi.19.2.75-82.

[2] Et-taya L., Ouslimane T., Benami A.. Numerical analysis of earth-abundant Cu. *Solar Energy*. 2020;201:827-835. doi:10.1016/j.solener.2020.03.070.

[3] Bhattarai S., Mhamdi A., Hossain I., Raoui Y.. A detailed review of perovskite solar cells: Introduction,

working principle, modelling, fabrication techniques, future challenges. *Micro and Nanostructures*. 2022;172:207450. doi:10.1016/j.micrna.2022.207450.

[4] Rana A. D., Pharne I. D., Bhargava K.. Numerical simulation of highly efficient double perovskite solar cell using SCAPS-1D. *Materials Today: Proceedings*. 2023;73:584-589. doi:10.1016/j.matpr.2022.11.110.

[5] Li J., Wang Q., Abate A.. Perovskite solar cells. *Perovskite Solar Cells*. 2019. doi:10.1016/B978-0-12-813337-8.00012-6.

[6] Al Qadri M. A., Sipahutar W. S., Khamidy N. I., Saputra I. S., Widianto E., Astuti W., others. Enhancing the Performance of MAPbI. *Journal of Electronic Materials*. 2024;53:6838-6849. doi:10.1007/s11664-024-11386-1.

[7] Al Qadri M. A., Nurfani E.. Effect of TiO. *Next Materials*. 2025;8:100537. doi:10.1016/j.nxmate.2025.100537.

[8] Al Qadri M. A., Nurfani E.. Effect of precursor molarity on the structural, morphological, and photovoltaic properties of MAPbI. *Materials Science and Engineering: B*. 2026;323:118686. doi:10.1016/j.mseb.2025.118686.

[9] Saputri H. E., Indriyani N., Sipahutar W. S., Saputra I. S., Asri R., Yuliantini L., others. Molarity-Controlled FAI Surface Passivation for Enhanced Photovoltaic Performance of MAPbI. 2026. doi:10.2139/ssrn.6455938.

[10] Widianto Eri, Mahendra Bhisma, Riswan Muhammad, Kusuma Frendy Jaya, Kardiman, Nurfani Eka, Pardede Indra, Nursam Natalita Maulani, Triyana Kuwat, Santoso Iman. Advancing perovskite solar cells: Optical characterization and performance enhancement via spectroscopic ellipsometry. *Journal of Science: Advanced Materials and Devices*. 2025;10:100881. doi:10.1016/j.jsamd.2025.100881.

[11] Battula R. K., Sudakar C., Bhyrappa P., Veerappan G., Ramasamy E.. Performance-stability correlation in MAPbI. *Optical Materials*. 2024;153:115538. doi:10.1016/j.optmat.2024.115538.

[12] Gordillo G., Torres O. G., Abella M. C., Peña J. C., Virguez O.. Improving the stability of MAPbI. *Journal of Materials Research and Technology*. 2020;9:13759-13769. doi:10.1016/j.jmrt.2020.09.095.

[13] Kim B., Kim M., Kim H., Jeong S., Yang J., Jeong M. S.. Improved Stability of MAPbI. *ACS Applied Materials & Interfaces*. 2022;14:35726-35733. doi:10.1021/acsami.2c08680.

[14] Liu D., Shao Z., Li C., Pang S., Yan Y., Cui G.. Structural Properties and Stability of Inorganic CsPbI. *Small Structures*. 2021;2:2000089. doi:10.1002/sstr.202000089.

[15] Wang Y., Chen Y., Zhang T., Wang X., Zhao Y.. Chemically Stable Black Phase CsPbI. *Advanced Materials*. 2020;32:2001025. doi:10.1002/adma.202001025.

[16] Tan X., Wang S., Zhang Q., Liu H., Li W., Zhu L., others. Stabilizing CsPbI. *Matter*. 2023;6:691-727. doi:10.1016/j.matt.2022.12.012.

[17] Hunde B. R., Woldeyohannes A. D.. Performance analysis and optimization of perovskite solar cell using SCAPS-1D and genetic algorithm. *Materials Today Communications*. 2023;34:105420. doi:10.1016/j.mtcomm.2023.105420.

[18] Aseena S., Abraham N., Suresh Babu V.. Optimization of layer thickness of ZnO based perovskite solar cells using SCAPS-1D. *Materials Today: Proceedings*. 2020;43:3432-3437. doi:10.1016/j.matpr.2020.09.077.

[19] Farshad S., Shojaei S., Khameneh S.. High-performance CsPbI. *Optics Communications*. 2022;512:128053. doi:10.1016/j.optcom.2022.128053.

[20] Chowdhury M. S., Shahahmadi S. A., Chelvanathan P., Tiong S. K., Amin N., Techato K., others. Effect of deep-level defect density of the absorber layer and n/i interface in perovskite solar cells by SCAPS-1D. *Results in Physics*. 2020;16:102839. doi:10.1016/j.rinp.2019.102839.

[21] Reyes A. C. P., Lázaro R. C. A., Leyva K. M., López J. A. L., Méndez J. F., Jiménez A. H. H., others. Study of a lead-free perovskite solar cell using CZTS as HTL to achieve a 20\% PCE by SCAPS-1D simulation. *Micromachines*. 2021;12:1508. doi:10.3390/mi12121508.

[22] Nurfani Eka, Kadja Grandprix T. M., Purbayanto Muhammad A. K., Darma Yudi. The role of substrate temperature on defects, electronic transitions, and dark current behavior of ZnO films fabricated by spray technique. *Materials Chemistry and Physics*. 2020;239:122065. doi:10.1016/j.matchemphys.2019.122065.

[23] Nurfani Eka, Kadja Grandprix T. M., Purbayanto Muhammad A. K., Darma Yudi. Origin of fast-response photocurrent in ZnO thin film. *Optical Materials*. 2018;82:70-76. doi:10.1016/j.optmat.2018.06.014.

[24] Zyoud S. H., Zyoud A. H., Ahmed N. M., Prasad A. R., Khan S. N., Abdelkader A. F. I., others. Numerical modeling of high conversion efficiency FTO/ZnO/CdS/CZTS/Mo thin film-based solar cells: Using SCAPS-1D software. *Crystals*. 2021;11:1468. doi:10.3390/cryst11121468.

[25] Fatema K., Arefin M. S.. Enhancing the efficiency of Pb-based and Sn-based perovskite solar cell by applying different ETL and HTL using SCAPS-1D. *Optical Materials*. 2022;125:112036. doi:10.1016/j.optmat.2022.112036.

[26] Srivastava V., Chauhan R. K., Lohia P.. Highly efficient cesium-based halide perovskite solar cell using SCAPS-1D software: Theoretical study. *Journal of Optics*. 2022. doi:10.1007/s12596-022-00946-5.

[27] Mortadi A., El Hafidi E., Monkade M., El Moznine R.. Investigating the influence of absorber layer thickness on the performance of perovskite solar cells: A combined simulation and impedance spectroscopy study. *Materials Science for Energy Technologies*. 2024;7:158-165. doi:10.1016/j.mset.2023.10.001.

[28] Rai M., Wong L. H., Etgar L.. Effect of Perovskite Thickness on Electroluminescence and Solar Cell Conversion Efficiency. *The Journal of Physical Chemistry Letters*. 2020;11:8189-8194. doi:10.1021/acs.jpclett.0c02363.

[29] Obi U. C., Sanni D. M., Bello A.. Effect of Absorber Layer Thickness on the Performance of Bismuth-Based Perovskite Solar Cells. *Semiconductors*. 2021;55:922-927. doi:10.1134/S1063782621040114.

[30] Chen J., Park N.-G.. Causes and Solutions of Recombination in Perovskite Solar Cells. *Advanced Materials*. 2019;31:1803019. doi:10.1002/adma.201803019.

[31] Ryu S., Ha N. Y., Ahn Y. H., Park J.-Y., Lee S.. Light intensity dependence of organic solar cell operation and dominance switching between Shockley–Read–Hall and bimolecular recombination losses. *Scientific Reports*. 2021;11:16781. doi:10.1038/s41598-021-96222-w.

[32] Sarritzu V., Sestu N., Marongiu D., Chang X., Masi S., Rizzo A., others. Optical determination of Shockley-Read-Hall and interface recombination currents in hybrid perovskites. *Scientific Reports*. 2017;7:44629. doi:10.1038/srep44629.

[33] Wolff C. M., Caprioglio P., Stolterfoht M., Neher D.. Nonradiative Recombination in Perovskite Solar Cells: The Role of Interfaces. *Advanced Materials*. 2019;31:1902762. doi:10.1002/adma.201902762.

[34] Dunfield S. P., Bliss L., Zhang F., Luther J. M., Zhu K., van Hest M. F. A. M., others. From Defects to Degradation: A Mechanistic Understanding of Degradation in Perovskite Solar Cell Devices and Modules. *Advanced Energy Materials*. 2020;10:1904054. doi:10.1002/aenm.201904054.

[35] Ahn N., Choi M.. Towards Long-Term Stable Perovskite Solar Cells: Degradation Mechanisms and Stabilization Techniques. *Advanced Science*. 2024;11:2306110. doi:10.1002/advs.202306110.

[36] Bisquert J., Juarez-Perez E. J.. The Causes of Degradation of Perovskite Solar Cells. *The Journal of Physical Chemistry Letters*. 2019;10:5889-5891. doi:10.1021/acs.jpclett.9b00613.